Dyes and Pigments 195 (2021) 109703

Contents lists available at ScienceDirect

Dyes and Pigments

journal homepage: www.elsevier.com/locate/dyepig

Positive temperature dependence of the electroluminescent performance in a colloidal quantum dot light-emitting diode

Mingrui Zhang [a], Feng Guo [a], Shiyun Lei [a], Tian Zhong [a], Biao Xiao [a,b,*], Cui Liu [a], Liang Wang [a], Jia Chen [a,b], Qingliang You [a,b], Jiyan Liu [a,b,**], Renqiang Yang [a,b,***]

[a] Key Laboratory of Optoelectronic Chemical Materials and Devices, Ministry of Education, School of Chemical and Environmental Engineering, Jianghan University, Wuhan 430056, Hubei, China

[b] Flexible Display Materials and Technology Co-Innovation Centre of Hubei Province, Jianghan University, Wuhan 430056, Hubei, China

ARTICLE INFO

Keywords:
Quantum dot light-emitting diode
Temperature-dependent electroluminescence
Thermionic emission model
Trap states

ABSTRACT

In this study, the temperature dependence of the dynamic behavior in colloidal quantum dot light-emitting diodes (QLEDs) in a wide temperature range (120 K–300 K) is investigated. The results demonstrate that the electroluminescent performance of the device is enhanced as the temperature rises. Particularly, the device current efficiency is improved and the turn-on voltage is lowered. In addition, the decline in temperature results in a blue-shift of the electroluminescence spectrum. Consequently, the charge injection barrier is studied using thermionic emission model and impedance spectroscopy, and the results show that this injection barrier increases when the temperature is elevated, leading to more difficult charge injection. Meanwhile, the charge transport study proves that the average charge lifetime in the device is prolonged at higher temperature, which is beneficial for the transport of charges. Furthermore, the analyses of the trap states and their distribution reveal that more trap states exist at low temperature, causing performance degradation in the device. The analysis and discussion in this work provide fundamental insights into the working mechanism of QLEDs and can be used to predict device performance under extreme operating conditions.

1. Introduction

Due to their many advantages such as low energy consumption, simple preparation process and good color rendering ability, colloidal quantum dot-based light-emitting devices (QLEDs) have received widespread attention in the fields of flat panel display and solid-state lighting [1–4]. By designing new quantum dot (QD) materials and/or optimizing the device structure, the highest external quantum efficiency (EQE) of red, green and blue quantum dot light-emitting diodes is either approaching or has exceeded 20 % [5–8]. In other words, in terms of luminous efficiency only, QLED has reached the requirements of commercialization. However, some other parameters such as stability of electroluminescence (EL) performance play decisive roles in the large-scale application of QLEDs as well. For a light-emitting device (LED) with high practical value, it must possess good environmental endurance, especially a wide operating temperature range. Therefore, it is of great significance to study the device luminous characteristics at different temperatures. In previous studies, great efforts have been made to explore the effect of temperature on the luminescence properties of various types of light-emitting diodes [9–12]. However, there are still uncertainties remaining in the temperature-performance relationship. For example, the device efficiency in the NPD-Alq_3 based organic light-emitting diode (OLED) is found to be increased when the temperature decreases in the range of 250 K–300 K, as reported in the literature [9]. While Edman et al. conversely reported that the current efficiency of Super Yellow-based OLED devices is independent of temperature between 293 K and 353 K [10]. The correlation between the luminescence performance and the temperature were also studied in the perovskite

* Corresponding author. Key Laboratory of Optoelectronic Chemical Materials and Devices, Ministry of Education, School of Chemical and Environmental Engineering, Jianghan University, Wuhan 430056, Hubei, China.

** Corresponding author. Key Laboratory of Optoelectronic Chemical Materials and Devices, Ministry of Education, School of Chemical and Environmental Engineering, Jianghan University, Wuhan 430056, Hubei, China.

*** Corresponding author. Key Laboratory of Optoelectronic Chemical Materials and Devices, Ministry of Education, School of Chemical and Environmental Engineering, Jianghan University, Wuhan 430056, Hubei, China.

E-mail addresses: biaoxiao@jhun.edu.cn (B. Xiao), liujiyan918@163.com (J. Liu), yangrq@jhun.edu.cn (R. Yang).

https://doi.org/10.1016/j.dyepig.2021.109703
Received 14 June 2021; Received in revised form 5 August 2021; Accepted 5 August 2021
Available online 8 August 2021

light-emitting diode. For instance, it is reported that LEDs based on $CsPbBr_3$ perovskite nanocrystals lost ~95 % of their initial room-temperature EL efficiency when operated at 393 K [11]. Whereas, based on the nanocrystalline materials of similar chemical composition, Li et al. achieved stable photon emission from room temperature to 373 K [12]. It should be pointed out that in the classic InGaN/GaN multiple-quantum-well light-emitting diodes, different temperature dependence rules of the EL intensity and peak energy have also been observed in green, blue, and ultraviolet (UV) devices [13]. In a word, the temperature dependence of device performance is very complicated, and even contradictory. As far as we know, temperature-dependent luminescent behaviors of colloidal quantum dot-based light emitting devices have seldom been investigated, which limits its application in non-room temperature fields. It should be noted that, although many works have studied the photoluminescence behavior of light-emitting quantum dots at different temperatures, their conclusions cannot be fully applied to electroluminescent QLEDs, since the mechanism of electroluminescence is fundamentally different from photoluminescence. The electroluminescence process is not only related to the light-emitting quantum dots, but also related to the complex physical processes during the electro-optic conversion [2,3,14]. In order to obtain a comprehensive understanding of the temperature-dependent electroluminescence in QLEDs, different factors, such as charge injection, transport and trap-related charge capture and release, which can affect the temperature dependence of QLEDs, should be involved and discussed in detail.

Herein, we report positive temperature dependence of electroluminescent performance in colloidal quantum dot light-emitting diode. In more detail, we found that the luminous efficiency of the device at low temperatures is significantly lower than that at room temperature. To clarify the mechanism, a detailed study on the charge injection and charge transport was carried out. The results show that temperature variation has opposite effects on these two processes: lowering the temperature will lead to a reduction in the charge injection barrier, which is beneficial to the injection of charges, while low temperature will also decrease the efficiency of charge transport. The Gaussian trap distribution model was used to quantitatively analyze the traps in the device, and we found that an increase in trap states at low temperatures is the main reason for the degradation of device performance. These results enable us to understand the impact of temperature on the performance of QLEDs.

2. Results and discussion

Dependence of the electroluminescent performance on temperature. In order to study the influence of temperature on the electroluminescence, QLEDs were constructed with a typical configuration of indium tin oxide (ITO)/poly-(ethylenedioxythiophene):poly(styrene

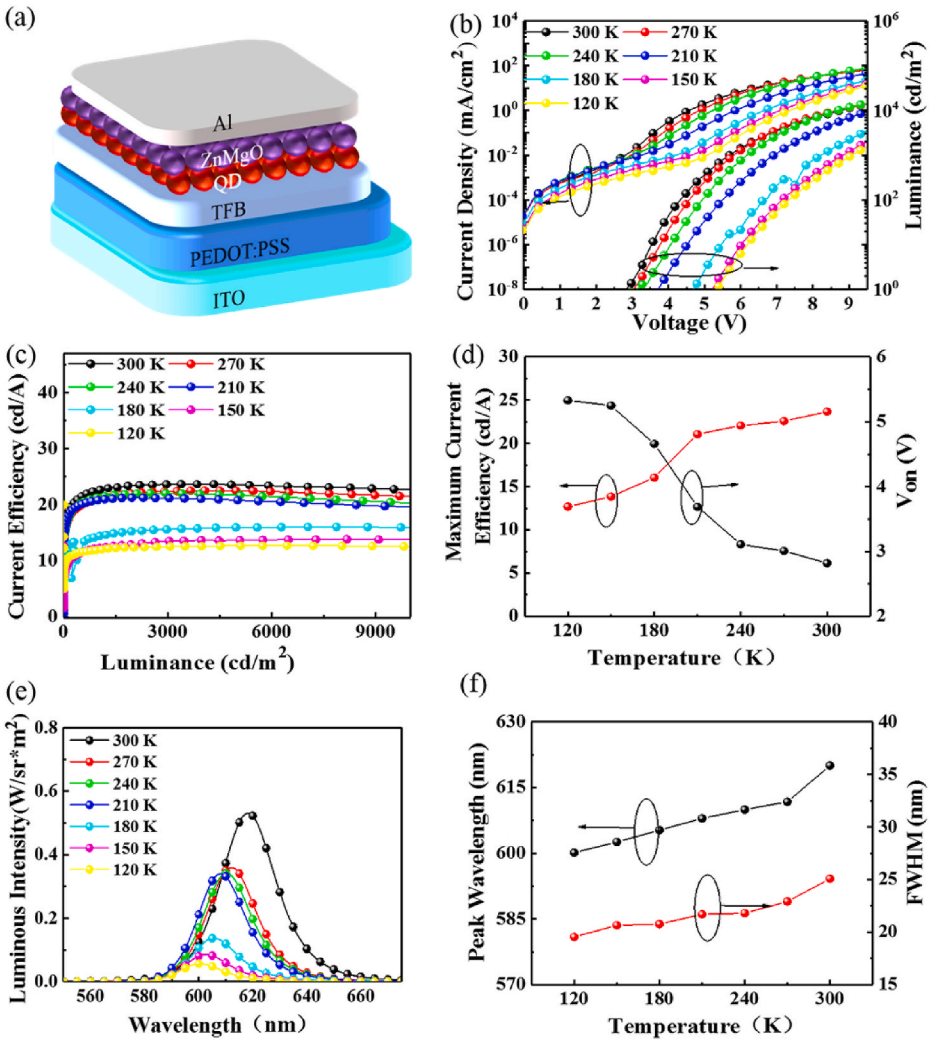

Fig. 1. (a) Schematic of the QLED device configuration. (b) Current density - voltage - luminance and (c) Current efficiency-luminance characteristics of the diode as functions of temperature. (d) The current efficiency and the turn-on voltage extracted from (b) and (c). (e) Electroluminescence spectra measured at various temperatures, the applied voltage is fixed at 6 V. (f) The peak wavelengths and the full width at half maxima (FWHM) at different temperatures.

sulfonate)(PEDOT:PSS)/poly(9,9-dioctylfluorene-co-*N*-(4-butylphenyl) diphenylamine) (TFB)/QDs/ZnMgO/Al. All layers were sequentially spin-coated onto the patterned ITO substrate except for the Al cathode, which was deposited via vacuum thermal evaporation. The device structure is illustrated in Fig. 1a. Fig. 1b and c present a series of current density-voltage-luminance (*J-V-L*) and current efficiency (CE, defined as *L/J*) - luminance curves of the red QLED at various temperatures. To ensure that the temperature is accurate, the devices were placed in a precise cryostat, in which the heat generated by the device will be taken away immediately by liquid nitrogen. As shown in Fig. 1b, both the current density and luminance decrease with lowering the temperature, similar to the behavior observed in OLEDs [15,16]. In those OLEDs, different from the current density and luminance, the CE increases with temperature decline. However, in this study, as illustrated in Fig. 1c, the current efficiency in the QLED demonstrates positive temperature dependence, which is opposite to that in OLEDs. Fig. 1d depicts the influence of temperature on the maximum CE and the turn-on voltage (V_{on}) of the device. In the temperature range of 120 K–300 K, the maximum CE of the device increases as the temperature rises. When the temperature is 120 K, the maximum CE of the device is 12.67 cd/A. As raising the temperature to 300 K, this value is greatly augmented to 23.67 cd/A, whereas the V_{on} declines significantly. The V_{on} and CE show opposite trends with temperature, and an increase in temperature is conducive to reducing the V_{on} of the device.

Electroluminescent spectrum is another important parameter for evaluating the performance of QLEDs. The temperature-dependent EL spectra of the QLED are plotted in Fig. 1e. It is found that the luminous intensity of the device decreases with the lowering of temperature, indicating that low temperature suppressed the luminescence performance of the device. This result is consistent with the aforementioned CE measurement. The peak position and the full width at half maximum (FWHM) data of the electroluminescence spectra in Fig. 1e are extracted and plotted in Fig. 1f. It is worth noting that when the temperature drops from 300 K to 120 K, the peak position shifts from 620 nm to 600 nm and the FWHM also decreases from 25.07 nm to 19.54 nm. This phenomenon reflects carrier relaxation into lower energy localized states, and the change in charge-recombination dynamics at low temperatures.

Charge injection and transport study. In order to gain in-depth understanding of the temperature dependence of the electroluminescent performance, charge injection and transport processes were investigated. The current-voltage curves at various temperatures were fitted by the thermionic emission model, which is one of the most used models in QLEDs [17,18]. As shown in Fig. 2a and b, both the plots of ln(*I*) vs $V^{1/2}$ and ln(I/T^2) vs $1/T$ show preferable linear relationships within the temperature and voltage range of measurement, suggesting the thermionic emission plays a dominating role during charge injection [19,20]. The thermionic emission can be expressed as [21].

$$I = I_0 \exp\left(\frac{qV}{nkT}\right)\left[1 - \exp\left(\frac{qV}{kT}\right)\right] \quad (1)$$

where q is the elementary charge, V is the applied bias, n is the ideality factor of the diode, k is Boltzmann constant, T is the temperature, and I_0 is the saturation current, which is given by:

$$I_0 = AA^*T^2\exp\left(-\frac{q\varphi_B}{kT}\right) \quad (2)$$

where Φ_B is the barrier height, and A is the effective area of the device, A^* is the effective Richardson constant. Using equations (1) and (2), the variation trend of the charge injection barrier in QLED with temperature can be calculated, which is shown in Fig. 2d. As illustrated in the figure, the charge injection barrier height is temperature-dependent and the barrier falls off with the decrease of temperature.

The charge injection process can also be monitored by impedance spectroscopy (IS). The Nyquist plots of the device at various temperatures are shown in Fig. 2c. The IS measurement was performed in the frequency range from 20 Hz to 10 MHz. The solid lines in Fig. 2c represent the fitting results derived from the equivalent circuit depicted in the inset of Fig. 2c. Details of the fitting parameters can be found in Table S1. The fitted curves match well with the experimental data, suggesting that the circuit model reflects the real circuit. In this model,

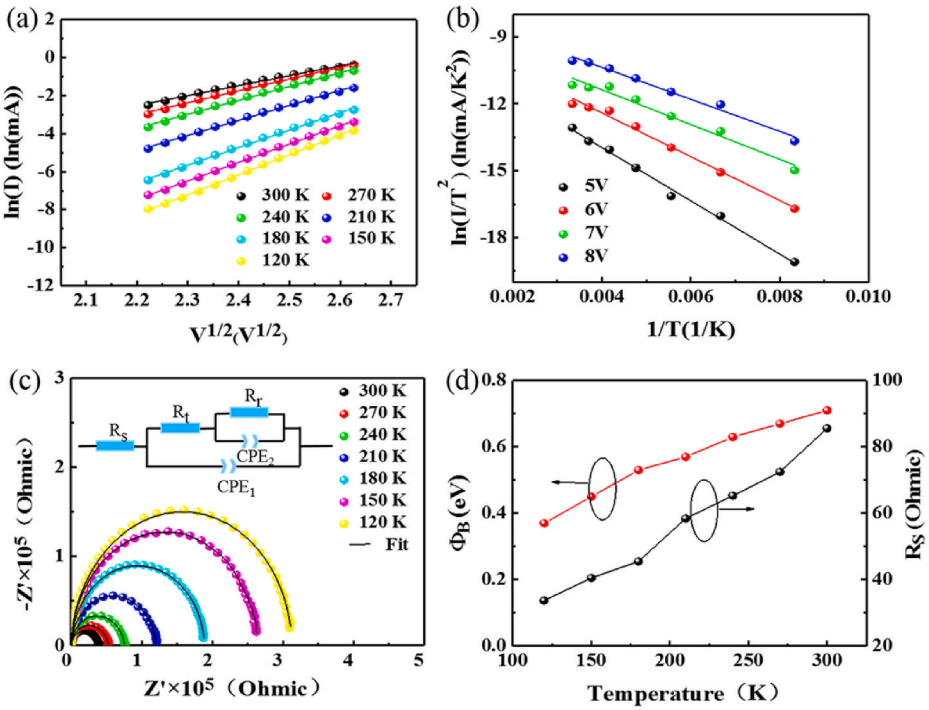

Fig. 2. (a) Typical current density-voltage curves plotted in a ln(*I*) vs $1/V^{1/2}$ form for different temperatures. (b) The correlation between ln(I/T^2) and $1/T$ at various applied voltages. The straight lines in (a) and (b) are linear fits to the experimental data. (c) Nyquist plots of the QLED at different temperatures. The fitting curves were obtained using the equivalent circuit shown in the inset of (c). (d) Extracted Φ_B and R_s values as functions of the temperature.

R_t and R_r are the transport and recombination resistances in the device. CPE_1 and CPE_2 are constant phase elements that are introduced into the circuit model instead of the capacitors to describe the imperfect physical processes. R_s represents the series resistance arising from a number of contact interfaces [22–25]. The larger the R_s, the more difficult the charge injection at the interface. Therefore, the value of R_s can be used to evaluate the charge injection capability at the interface. As shown in Fig. 2d, when the temperature drops from 300 K to 120 K, the value of R_s decreases from 85.6 Ω to 33.7 Ω. In other words, the charge injection capability is enhanced at low temperature. It is worth noting that this inference is consistent with the fitting results of thermionic emission model.

To clarify the effects of temperature on the charge transport properties in QLEDs, single-carrier devices were fabricated and their current density-voltage characteristics were investigated at different temperatures. Fig. 3a and b show the current density-voltage curves of the electron- and hole-only devices at different temperatures. In the electron- and hole-only devices, the current characteristics represent the electron and hole transport behavior for the devices because holes are blocked by the ZnMgO layer and electrons blocked by the TFB layer [26],respectively. As depicted in Fig. 3a and b, for both electron- and hole-only devices, raising the temperature causes a noticeable augmentation in the current density. In addition, Fig. 3c illustrates that elevating the temperature leads to a decrease in charge transport resistance R_t and an increase in average charge lifetime (τ_{ave}), indicating that charges are easier to transport in the device at a higher temperature. These phenomena are consistent with the results observed in other devices that based on disordered semiconductors [27,28].

Identification of charge transport traps and their impact on the electroluminescent performance. Device performance in optoelectronic devices is strongly influenced by trap states [29,30]. Yet, the role of traps in QLEDs remains mostly overlooked. The origin of trap states in QDs has been correlated to the vacancies and dangling bonds which are created in the surface modification procedure [31]. Besides, the long organic ligands in the QD solid film may cause the generation of trapping sites for charge transport between neighboring QDs [32]. Therefore, capacitance-frequency-temperature measurement, which is also known as thermal admittance spectroscopy, was carried out to investigate the trap states. Fig. 4a shows the capacitance of the diode at temperatures between 120 K and 300 K. Within the high-frequency range (10^4–10^6 Hz), charge carriers are not able to respond to the applied signal, the capacitance value is basically a constant, corresponding to the geometric capacitance (C_{geo}) of the device. Thus, the relative dielectric constant (ε_r) can be obtained by a simple equation, $C_{geo} = \varepsilon_r\varepsilon_0/d$, where ε_0 is the permittivity of free space, and d is the distance between the two electrodes. Consequently, upon experimentation and calculations, the organic/inorganic multilayer presents an apparent relative dielectric constant of 7.68, which is in good agreement with those in the previous reports [33,34]. In the low-frequency region ($<10^3$ Hz), the capacitance of the device becomes larger as the temperature rises. The reason for this phenomenon is that the charges are released from the trap states at a higher temperature due to higher electron energy, leading to charge accumulation and an increase in capacitance [35,36]. Therefore, the capacitance growth behavior is indicative of trap states.

In order to further study the effect of traps on the device performance, the method proposed by Walter et al. was applied to study the DOS in the QLEDs at various temperatures [37]. Gaussian type trap distribution function was employed to fit the experimental results, and the results are shown in Fig. 4b. As the temperature rises, the energy difference between the trap state and the valence band ($E\text{-}E_v$) becomes larger, and the trap density (n_t) in the device decreases (shown in Fig. S1). These phenomena are reasonable because the trapped electrons possess higher average energy at elevated temperatures and are more likely to change from a “frozen state” to an “activated state”. That is, increasing the temperature increases the energy of the trapped charges, making them easier to escape from the trapping sites and contribute to the radiative charge recombination, resulting in higher luminous efficiency. It is worth noting that the decrease of trap density with the increase of temperature has also been observed in PbS-based quantum dots [38]. Another interesting phenomenon in Fig. 4b is the broadening of the DOS distribution at elevated temperatures (larger σ values at higher temperatures, as shown in Figure S1), which is consistent with the widening of the FWHM of the electroluminescence spectra shown in Fig. 1f.

Fig. 4c shows the photoluminescence (PL) spectra of the quantum dot film at various temperatures. An increase in PL intensity with lowering of the temperature is observed, indicating the quenching of nonradiative recombination pathways in the quantum dots. The opposite trends of PL and EL intensity with temperature demonstrates that the influence of temperature on the quantum dot itself is less than the influence on the behavior of charge transport. One remaining issue is that the luminescence spectrum blue-shifts as the temperature decreases. Therefore, temperature-dependent photoluminescence spectroscopy was employed to determine the bandgap energy of the quantum dots [39]. Fig. 4d depicts the correlation between the bandgap of the quantum dot and the temperature. Apparently, with the fall in temperature, the bandgap of the quantum dot is monotonously increased. Therefore, we believe that the blue-shift of the electroluminescent spectrum at low temperatures is ascribed to the bandgap expansion of quantum dots. This result can be understood as follows: the larger the energy difference between the bottom of conduction band and the top of valence band, the higher the photon energy emitted. The underlying mechanism for the widening of bandgap is not clearly clarified yet, possible reason is the shrinkage of the lattice of QDs, or may be caused by the attenuation of electroacoustic coupling at lower temperatures [40,41].

3. Conclusions

In summary, a colloidal quantum dot-based light-emitting diode was

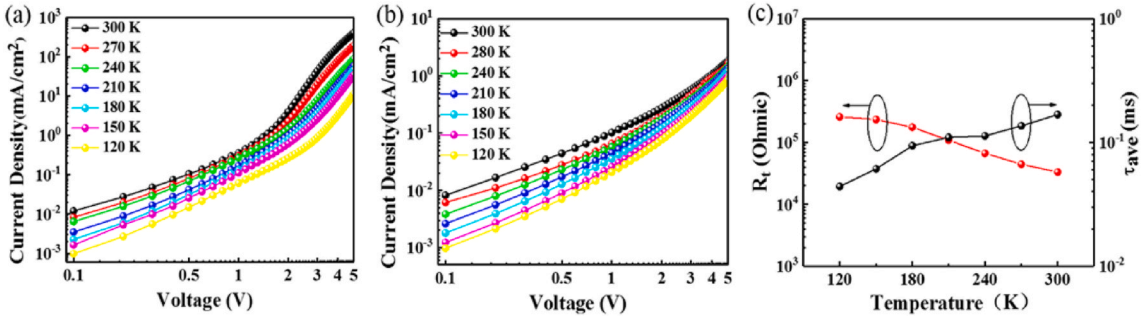

Fig. 3. Current density-voltage curves of the electron-only (a) and hole-only (b) devices. Configurations for the electron- and hole-only device are ITO/ZnMgO/QD/ZnMgO/Al and ITO/PEDOT:PSS/TFB/QD/MoO_3/Al, respectively. (c)Transport resistance R_t and average charge lifetime τ_{ave} as functions of temperature.

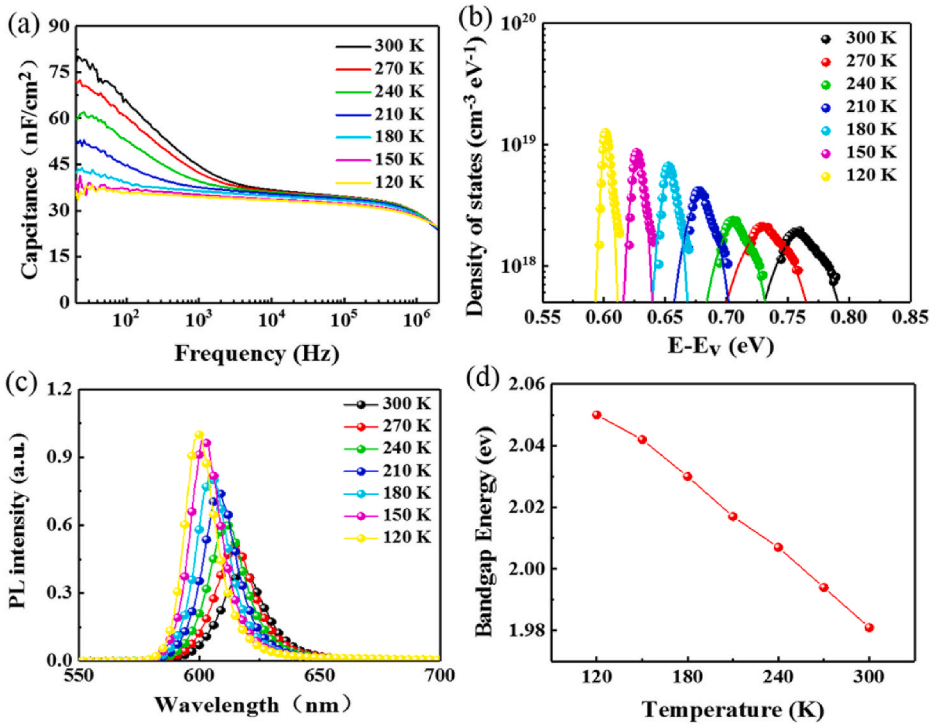

Fig. 4. (a) Capacitance measurements performed at temperatures ranging from 120 K to 300 K. (b) Density of states (DOS) profiles at different temperatures. The solid lines are fitting curves from the Gaussian trap state distribution model: $g_t(E_\omega) = \frac{n_t}{\sqrt{2\pi}\sigma} exp\left[-\frac{(E_0-E_\omega)^2}{2\sigma^2}\right]$, where n_t is the trap density, σ is the width of the Gaussian type trap distribution, E_0 is the average energy. (c) Photoluminescent spectra of the quantum dot film under different temperatures, the excitation wavelength of photoluminescence test is 450 nm. (d) The variation of bandgap with temperature.

fabricated and its electroluminescence performance was studied in a wide temperature range from 120 K to 300 K. The current efficiency of the device is improved as the temperature rises, while the turn-on voltage presents an opposite trend, that is, when the temperature increases, the turn-on voltage decreases. In addition, the lowering in temperature will cause a blue-shift of the electroluminescence spectrum. Thermionic emission model and impedance spectroscopy were employed to investigate the charge injection barrier. As a result, the charge injection barrier height is temperature-dependent and the diode has a larger charge injection barrier at high temperatures. Charge transport study demonstrates that raising temperature leads to a lengthened average charge lifetime which is beneficial for charge transport. Through analyzing the trap states and their distribution in the device, it is found that the augmentation in trap states makes a great contribution to the device performance degradation at low temperatures. This work shows important significance for understanding the working mechanism of QLEDs at different temperatures.

4. Methods

Materials: The ITO substrates with a sheet resistance of ca. 12 Ω sq^{-1} were purchased from CSG Holding Co., Ltd. The PEDOT:PSS aqueous solution (Clevios P VP AI 4083) and TFB were purchased from H. C. Stark Inc. and Luminescence Technology Corp. (Lumtec), respectively. The QDs and ZnMgO nanoparticles were provided by Poly Opto Electronics Co., Ltd (POE). All the materials were used directly without further purification unless stated otherwise.

Device fabrication. The device structure was ITO/PEDOT:PSS/TFB/QDs/ZnMgO/Al. Pre-patterned ITO glass substrates were first cleaned using consecutive ultrasonication in acetone, detergent, deionized water, and isopropyl alcohol. Following that, the substrates were treated with oxygen plasma for 5 min, and then a 40 nm-thick PEDOT: PSS film was obtained by spin-coating on the ITO-coated glass. The substrates were subsequently dried at 150 °C in air. After that, the hole transporting material TFB (10 mg/mL) was spin-casted at 3000 rpm for 30 s and baked at 120 °C for 10 min in a N_2-glovebox. QD solution with a total concentration of 30 mg/mL in octane was spin-casted at 2000 rpm and baked at 100 °C for 10 min. ZnMgO nanoparticles, dispersed in ethanol with a concentration of 30 mg/mL, were spin-coated as electron transport layer at 3000 rpm and baked at 100 °C for 10 min. To complete the device, a 70 nm thick layer of Al electrode was thermally evaporated in a vacuum chamber at 1×10^{-5} Pa.

Characterizations. The current density-voltage-luminance characteristics were measured using a Keithley 2450 source-meter and a Konica Minolta luminance meter LS-150. The electroluminescence spectra were collected using a Topcon SR-UL2 Spectroradiometer. The photoluminescence spectra were obtained using a fluorescence spectrometer (Edinburgh, FLS 920). The capacitance spectra were recorded using an impedance analyzer (Keysight, E4990A). During the characterizations, a low temperature environment was provided by a cryostat system (Janis, ST-100).

Author contribution statement

M. Z and B.X. conceived the idea and designed the experiments. M. Z. fabricated and characterized the devices. F. G., S. L. and T. Z. conducted impedance characterizations. C. L., L. W. and J. C. synthesized the QDs and ZnMgO nanoparticles. B. X., Q. Y., J. L. and R. Y. coordinated and directed the study. All authors contributed to manuscript preparation, data analysis and interpretation, and discussed the results.

Declaration of competing interest

The authors declare that they have no known competing financial interests or personal relationships that could have appeared to influence the work reported in this paper.

Acknowledgements

The authors are deeply grateful to the Natural Science Foundation of China (52073122 and 51773220), the project of state guiding regional development for Hubei province (2019ZYYD005).

Appendix A. Supplementary data

Supplementary data to this article can be found online at https://doi.org/10.1016/j.dyepig.2021.109703.

References

[1] Yang Y, Zheng Y, Cao W, Titov A, Hyvonen J, Manders JR, Xue J, Holloway PH, Qian L. High-efficiency light-emitting devices based on quantum dots with tailored nanostructures. Nat Photonics 2015;9:259–66.

[2] Dai X, Deng Y, Peng X, Jin Y. Quantum-dot light-emitting diodes for large-area displays: towards the dawn of commercialization. Adv Mater 2017;29(14):1607022.

[3] Moon H, Lee C, Lee W, Kim J, Chae H. Stability of quantum dots, quantum dot films, and quantum dot light-emitting diodes for display applications. Adv Mater 2019;31(34):1804294.

[4] Shen H, Gao Q, Zhang Y, Lin Y, Lin Q, Li Z, Chen L, Zeng Z, Li X, Jia Y, Wang S, Du Z, Li LS, Zhang Z. Visible quantum dot light-emitting diodes with simultaneous high brightness and efficiency. Nat Photonics 2019;13(3):192–7.

[5] Wang L, Lin J, Hu Y, Guo X, Lv Y, Tang Z, Zhao J, Fan Y, Zhang N, Wang Y, Liu X. Blue quantum dot light-emitting diodes with high electroluminescent efficiency. ACS Appl Mater Interfaces 2017;9(44):38755–60.

[6] Dai X, Zhang Z, Jin Y, Niu Y, Cao H, Liang X, Chen L, Wang J, Peng X. Solution-processed, high-performance light-emitting diodes based on quantum dots. Nature 2014;515(7525):96–9.

[7] Manders JR, Qian L, Titov A, Hyvonen J, Tokarz-Scott J, Acharya KP, Yang Y, Cao W, Zheng Y, Xue J, Holloway PH. High efficiency and ultra-wide color gamut quantum dot LEDs for next generation displays. J Soc Inf Disp 2015;23(11):523–8.

[8] Jia H, Wang F, Tan Za. Material and device engineering for high-performance blue quantum dot light-emitting diodes. Nanoscale 2020;12(25):13186–224.

[9] Park J, Kawakami Y. Temperature-dependent dynamic behaviors of organic light-emitting diode. J Disp Technol 2006;2(4):333–40.

[10] Ràfols-Ribé J, Gracia-Espino E, Jenatsch S, Lundberg P, Sandström A, Tang S, Larsen C, Edman L. Elucidating deviating temperature behavior of organic light-emitting diodes and light-emitting electrochemical cells. Elucidating deviating temperature behavior of organic light-emitting diodes and light-emitting electrochemical cells. Adv. Opt. Mater. 2020;9(1):2001405.

[11] Shi Z, Li S, Li Y, Ji H, Li X, Wu D, Xu T, Chen Y, Tian Y, Zhang Y, Shan C, Du G. Strategy of solution-processed all-inorganic heterostructure for humidity/temperature-stable perovskite quantum dot light-emitting diodes. ACS Nano 2018;12(2):1462–72.

[12] Liu M, Wan Q, Wang H, Carulli F, Li L. Suppression of temperature quenching in perovskite nanocrystals for efficient and thermally stable light-emitting diodes. Nat Photonics 2021;15:379–85.

[13] Cao XA, Leboeuf SF, Rowland LB, Liu H. Temperature-dependent electroluminescence in InGaN/GaN multiple-quantum-well light-emitting diodes. J Electron Mater 2003;32(5):316–21.

[14] Pietryga JM, Park YS, Lim J, Fidler AF, Bae WK, Brovelli S, Klimov VI. Spectroscopic and device aspects of nanocrystal quantum dots. Chem Rev 2016;116(18):10513–622.

[15] Shen Z, Burrows PE, Bulovic V, McCarty DM, Thompson ME, Forrest SR. Temperature dependence of current transport and electroluminescence in vacuum deposited organic light emitting devices. Jpn J Appl Phys 1996;35(3B):L401–4.

[16] Saha SK, Juang FS, Su YK. Temperature dependence of the electroluminescence for tris(8-hydroxy) quinoline aluminum (Alq^3) light emitting diode. IEEE J Quant Electron 2001;37(6):807–12.

[17] Tu Y, Wang S, Zhang Y, Chen L, Fang Y, Du Z. Balanced carrier injection of quantum dots light-emitting diodes: the case of interface barrier of bilayer ZnO electron transport layer. Nanotechnology 2018;29(48):485203.

[18] Kim S-K, Kim Y-S. Charge carrier injection and transport in QLED layer with dynamic equilibrium of trapping/de-trapping carriers. J Appl Phys 2019;126(3):035704.

[19] Li J-C, Wang D, Ba D-C. Effects of temperature and light Illumination on the current-voltage characteristics of molecular self-assembled monolayer junctions. J Phys Chem C 2012;116(20):10986–94.

[20] Appenzeller J, Radosavljevi M, Knoch J, Avouris P. Tunneling versus thermionic emission in one-dimensional semiconductors. Phys Rev Lett 2004;92(4):048301.

[21] Kumar S, Katharria YS, Kumar S, Kanjilal D. Temperature-dependence of barrier height of swift heavy Ion Irradiated Au/n-Si Schottky structure. *Solid-state electron*. Solid State Electron 2006;50(11–12):1835–7.

[22] Xiao B, Zhang M, Yan J, Luo G, Gao K, Liu J, You Q, Wang H-B, Gao C, Zhao B, Zhao X, Wu H, Liu F. High efficiency organic solar cells based on amorphous electron-donating polymer and modified fullerene acceptor. Nano Energy 2017;39:478–88.

[23] Lin X, Wu X, Zheng J, Rui H, Zhang Z, Hua Y, Yin S. Enhanced performance of green perovskite quantum dots light-emitting diode based on Co-doped polymers as hole transport layer. IEEE Electron Device Lett 2019;40(99):1479–82.

[24] Zhao W, Xie L, Yi Y-Q-Q, Chen X, Hu J, Su W, Cui Z. Optimizing the central steric hindrance of cross-linkable hole transport materials for achieving highly efficient RGB QLEDs. Mater. Chem. Front. 2020;4(11):3368–77.

[25] Chulkin P, Vybornyi O, Łapkowski M, Skabara, P J, Data P. Impedance spectroscopy of OLEDs as a tool for estimating mobility and the concentration of charge carriers in transport layers. J Mater Chem C 2018;6(5):1008–14.

[26] Wang F, Sun W, Liu P, Wang Z, Zhang J, Wei J, Li Y, Hayat T, Alsaedi A, Tan Za. Achieving balanced charge injection of blue QuantumDot light-emitting diodes through transport layer doping strategies. J Phys Chem Lett 2019;10(5):960–5.

[27] Craciun NI, Wildeman J, Blom PWM. Universal arrhenius temperature activated charge transport in diodes from disordered organic semiconductors. Phys Rev Lett 2008;100(5):056601.

[28] Slade TJ, Grovogui JA, Kuo JJ, Anand S, Bailey TP, Wood M, Uher C, Snyder GJ, Dravid VP, Kanatzidis MG. Understanding the thermally activated charge transport in $NaPbmSbQm^{+2}$ (Q = S, Se, Te) thermoelectrics: weak dielectric screening leads to grain bboundary dominated charge carrier scattering. Energy Environ Sci 2020;13(5):1509–18.

[29] Zhang M, Guo F, Zhou Q, Zhong T, Xiao B, Zou L, You Q, You B, Li Y, Liu X, Liu H, Yan J, Liu J. Enhanced performance through trap states passivation in quantum dot light emitting diode. J Lumin 2021;234:117946.

[30] Gregg, Brian A. Transport in charged defect-rich π-conjugated polymers. J Phys Chem C 2009;113(15):5899–901.

[31] Wang R, Shang Y, Kanjanaboos P, Zhou W, Ning Z, Sargent EH. Colloidal quantum dot ligand engineering for high performance solar cells. Energy Environ Sci 2016;9(4):1130–43.

[32] Brown PR, Kim D, Lunt RR, Zhao N, Bawendi MG, Grossman JC, Bulović V. Energy level modification in lead sulfide quantum dot thin films through ligand exchange. ACS Nano 2014;8(6):5863–72.

[33] Singh UB, Dhar R, Pandey AS, Kumar S, Dabrowski R, Pandey MB. Electro-optical and dielectric properties of CdSe quantum dots and 6CHBT liquid crystals composites. AIP Adv 2014;4(11):117112.

[34] Yang Y, Guo W, Wang X, Wang Z, Qi J, Zhang Y. Size dependence of dielectric constant in a single pencil-like ZnO nanowire. Nano Lett 2012;12(4):1919–22.

[35] Blauth C, Mulvaney P, Hirai T. Negative capacitance as a diagnostic tool for recombination in purple quantum dot LEDs. J Appl Phys 2019;125(19):195501.

[36] Bozyigit D, Volk S, Yarema O, Wood V. Quantification of deep traps in nanocrystal solids, their electronic properties, and their influence on device behavior. Nano Lett. Nano Lett. 2013;13(11):5284–8.

[37] Carr JA, Chaudhary S. On the Identification of deeper defect levels in organic photovoltaic devices. J Appl Phys 2013;114(6):593–7.

[38] Jin Z, Wang A, Zhou Q, Wang Y, Wang J. Detecting trap states in planar PbS colloidal quantum dot solar cells. Sci Rep 2016;6(1):37106.

[39] Webster PT, Riordan NA, Liu S, Steenbergen EH, Synowicki RA, Zhang YH, Johnson SR. Measurement of InAsSb bandgap energy and InAs/InAsSb band edge positions using spectroscopic ellipsometry and photoluminescence spectroscopy. J Appl Phys 2015;118(24):245706.

[40] Ye C, Fang X, Wang M, Zhang L. Temperature-dependent photoluminescence from elemental sulfur species on ZnS nanobelts. J Appl Phys 2006;99(6):063504.

[41] Pejova B, Abay B, Bineva I. Temperature dependence of the band-gap energy and sub-band-gap absorption tails in strongly quantized ZnSe nanocrystals deposited as thin films. J Phys Chem C 2010;114(36):15280–91.

Supporting Information

Positive Temperature Dependence of the Electroluminescent Performance in Colloidal Quantum Dot Light-Emitting Diode

*Mingrui Zhang[a], Feng Guo[a], Shiyun Lei[a], Tian Zhong[a], Biao Xiao[*a,b], Liwen Hu[a,b], Cui Liu[a], Liang Wang[a], Jia Chen[a,b], Qingliang You[a,b], Jiyan Liu[*a,b], Renqiang Yang[*a,b]*

[a] Key Laboratory of Optoelectronic Chemical Materials and Devices, Ministry of Education, School of Chemical and Environmental Engineering, Jianghan University, Wuhan 430056, Hubei, China

[b] Flexible Display Materials and Technology Co-Innovation Centre of Hubei Province, Jianghan University, Wuhan 430056, Hubei, China

Table S1. Parameters used to fit the impedance spectra.

	R_s (Ω)	R_t (Ω)	R_r (Ω)	$CPE_{2\text{-}T}$ (F)	$CPE_{2\text{-}P}$	$CPE_{1\text{-}T}$ (F)	$CPE_{1\text{-}P}$	τ (s)
300K	85.6	33083	5993	2.8E-07	0.75	2.11E-09	0.97	1.72E-03
270K	72.5	44465	8524	1.6E-07	0.77	2.01E-09	0.98	1.41E-03
240K	65.3	66830	11256	1.0E-07	0.8	1.91E-09	0.98	1.15E-03
210K	58.4	108300	11892	9.4E-08	0.82	1.87E-09	0.98	1.11E-03
180K	45.5	176100	13235	7.1E-08	0.85	1.77E-09	0.98	9.35E-04
150K	40.5	234620	29819	2.1E-08	0.87	1.67E-09	0.98	6.11E-04
120K	33.7	258790	53811	8.2E-09	0.91	1.56E-09	0.99	4.34E-04

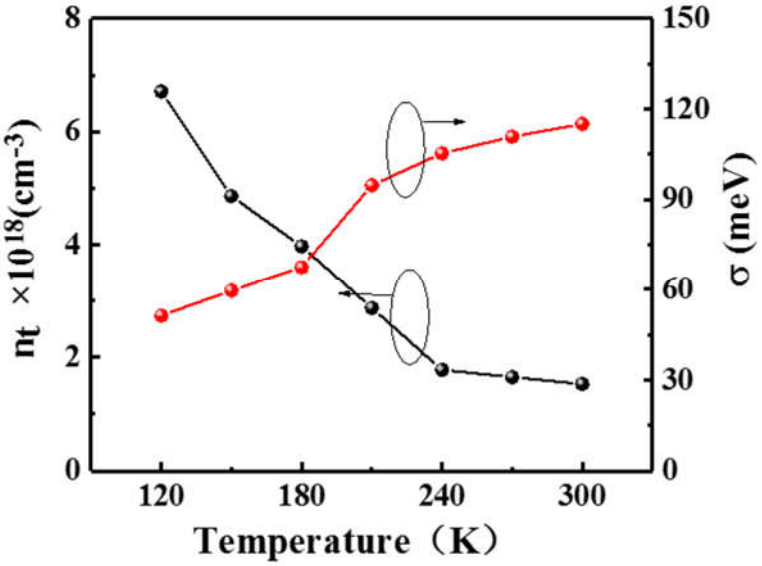

Figure S1. The σ value and trap density (n_t) in device as functions of temperature.